Morphing Thickness in Airfoils using Pneumatic Flexible Tubes and Kirigami Honeycomb

Jian Sun[1,2], Fabrizio Scarpa[2*], Jinsong Leng[1*]

[1] Center for Composite Materials and Structures, Harbin Institute of Technology, Harbin, China;
[2] Advanced Composites Centre for Innovation and Science (ACCIS), University of Bristol, Bristol, UK
*Corresponding author. Email: lengjs@hit.edu.cn, f.scarpa@bristol.ac.uk

Abstract

The work describes, a concept to morph the thickness of airfoils using a combination of Pneumatic Flexible Tubes (PFTs) within a Kirigami honeycomb configuration representing the wingbox structure. The configuration of the honeycomb/inflatable tube structure is composed by a pair of flexible tubes sandwiched between two custom honeycomb layouts. At zero input pressure the tube assumes a sinusoidal shape, which is reduced to a straight configuration and increase of the airfoil thickness when pressure is applied. An analytical model is developed to consider the actuation authority and thickness change provided by the system proposed. The results are benchmarked against experimental tests carried out on a reduced-scale demonstrator.

Keywords: Morphing Airfoil, Modelling, Inflatable Structure

NOMENCLATURE

P	Input pressure in the tube
a	Length of the side of hexagonal honeycomb
b	Distance between the upper and lower surface in the section of the compressed tube
s	Distance between the upper and lower honeycomb
c	Length of upper/lower surface in the section of the compressed tube
A	Amplitude of the sinusoidal curves
ω	Frequency of the sinusoidal curves
t_1,t_2	Offset Angle of the sinusoidal curves
B_1,B_2	Constant term of the sinusoidal curves
k	Gradient of the curve of s-b
B_3	Constant term of the curve of s-b
R	Outside radius of the semicircle of the tube
R_0	Original outside radius of the tube
t	Thickness of the tube
F_t	Shearing force on the two sides of semicircle unit
F_{t0}	Shearing force on the two sides of semicircle unit while the tube is a

	circle
M	Moment on the two sides of semicircle unit
ρ	Central radius of the semicircle unit
ρ_0	Original central radius of the semicircle unit
E	Young's Modules of the tube
I	Rotary inertia of the semicircle unit about x axis
w	Valid width of the semicircle unit
F_R	Recovery force of a tube caused by the circle structure
F_S	Recovery force of 1/4-period in a tube caused by stress
Δx	Increment in x direction
ε	Strain at x position
ΔF_S	Recovery force occurring at x position
A_{circle}	Tube's area in loop section
F_P	Force referring to input pressure
L	Action length of the input pressure for a tube
G	Loading force
P	Input pressure in the tube

1. INTRODUCTION

During the last two decades morphing technologies have demonstrated their capability to provide significant enhancement of the aircraft performance and broadening of the related flight envelope [1-3]. Several types of morphing techniques have been developed in recent years, and examples span from folding technologies for morphing wingtips to adaptive twist and variable camber [4-6]. The performance of a wing in a specific flight condition depends also on geometry properties of an airfoil provided by the maximum camber of the mean line and thickness distribution along the chord [7]. A thick wing performs more efficiently from the aerodynamic point of view at low speeds, while a thin wing is adapted to high speed flight [8, 9]. If the thickness of the airfoil can vary in a controllable way over the chord length, the aircraft can have a larger flight envelope and meet the demands of multiple missions [10]. An example of this concept is the morphing airfoil wing prototype based on shape memory alloys (SMA) actuators designed for subsonic cruise flight conditions, which has been tested in a subsonic wind tunnel [11].

Honeycomb and cellular structures are extensively used in airframe and sandwich applications for their high specific shear and bending stiffness, and recently have been proposed to morphing applications due to their compliance [12-14]. In morphing applications, the honeycomb does not change shape by itself, but needs the use of smart material within its core, like in the cases of SMA [15, 16] or Shape Memory Polymers (SMP) [17]. An alternative concept to create an adaptive honeycomb consists in using pressured fluid inside the cells. Variable camber wings have been already designed based on the use of a pneumatic pressurised honeycomb to obtain an adaptive configuration by applying either a uniform [18] or differential pressures at different cells locations [19, 20]. Pressured flexible tubes can also be used within the honeycombs or in segmented structures, such as prosthetic hands [21], robotic platforms [22-24], and biomimetic beam-steering antenna concepts [25, 26].

The paper describes a new morphing airfoil thickness concept based on the use of a Kirigami hexagonal honeycomb supporting an inflatable tube structure, which provides the shape change of the wingbox. Kirigami is the ancient Japanese art of folding and cutting paper spread in Asia since the 17th century, and it is particularly apt to build cellular structures with complex shapes using different types of thermosets and thermoplastics composites [27-30], as well as other metal substrates. An analytical model based on the geometry of the tube and approximations of the output force behaviour of the tube itself is presented. A demonstrator of the morphing inflatable honeycomb structure has also been produced, showing a general good agreement with the predictions provided by the model in terms of displacement-pressure actuation. A prototype of morphing airfoil has also been fabricated to further demonstrate the feasibility of the concept.

2. Morphing thickness in airfoil Concept

The morphing thickness airfoil structure consists in a cellular wingbox with Pneumatic Flexible Tubes (PFTs) as actuators (Figure 1). The tubes are installed horizontally between the upper and lower hexagonal honeycomb wingbox. When the pressure inside the tube is zero, the tube is contracted to follow an approximate sinusoidal shape. The input pressure in the inflatable tubes can control the thickness of the wing section. In the demonstrator developed in this work, a polyurethane (PU) foam filler is used to fill the cellular wingbox to increase the in-plane stiffness and guarantee a smooth change of the thickness to follow the aerodynamic shape.

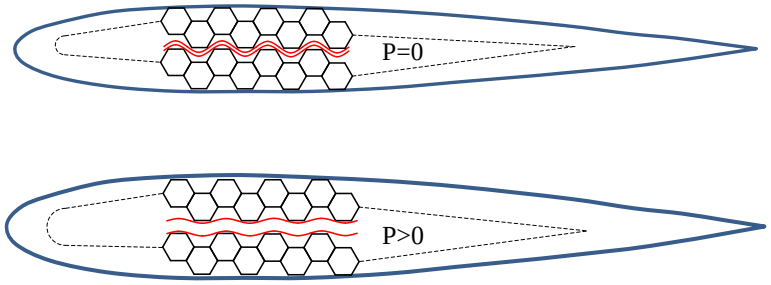

Figure 1. Schematic of the morphing thickness airfoil concept

3. Modeling

3.1 Geometric Model

Figure 2 shows a schematic representation of the unit cell of the morphing structure. The black lines represent the edge of hexagonal honeycomb cell, while the blue lines show the upper and lower surface of the tube sandwiched inside the cell. The model is developed following four assumptions:

(1) The tube is assumed to be symmetric with respect to its centerline after compression. The final upper and lower surfaces of the tube are flat, while the left and right surfaces are considered as semicircles. There is no contact inside the tube.

(2) Before compression (actuation) the upper and lower surfaces are sinusoidal.
(3) No sliding is present between the tubes and the honeycomb.
(4) The honeycomb is considered to simply transfer the load, and acts as a rigid body during the deformation of the tubes.

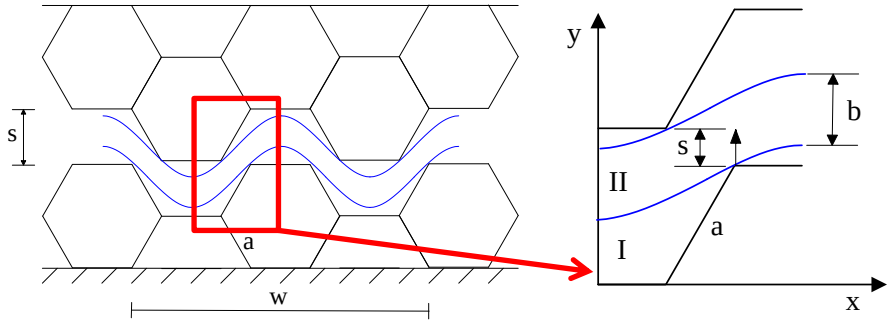

Figure 2. Morphing structure unit in rectangular coordinates

The two curves defining the shape of the tubes are described with the following equations:

$$y_I = A\sin(\omega x + t_1) + B_1 \tag{1}$$

$$y_{II} = A\sin(\omega x + t_2) + B_2 \tag{2}$$

Where $\omega = \frac{2\pi}{3a}$ and $t_1 = t_2 = -\frac{\pi}{2}$.

The upper curve passes through point $\left(a, \frac{\sqrt{3}}{2}a\right)$, therefore the term $B_1 = \frac{\sqrt{3}}{2}a - \frac{A}{2}$ is constant. The point $\left(\frac{a}{2}, s + \frac{\sqrt{3}}{2}a\right)$ belongs to the lower curve, as a consequence the value of B_2 is $B_2 = s + \frac{\sqrt{3}}{2}a + \frac{A}{2}$.
By inspection the following relation holds:

$$b = B_2 - B_1 = s + A \tag{3}$$

Assuming that a linear relationship exists between the terms *b* and *s*:

$$b = ks + B_3 \tag{4}$$

When $s = 2R_0, b = 2R_0$ and $s = -\frac{\sqrt{3}}{2}a, b = 0$, the coefficients *k* and B_3 assume the following forms:

$$k = \frac{2R_0}{2R_0 + \frac{\sqrt{3}}{2}a}, B_3 = \frac{\sqrt{3}}{2}ka \tag{5}$$

From observing Figure 3, the outside radius of the semicircle can be described as:

$$R = b/2 \tag{6}$$

The length of the straight line is obtained as:

$$c = \frac{2\pi R_0 - \pi R - \pi R}{2} = \pi\left(R_0 - \frac{b}{2}\right) \tag{7}$$

The relationships between the terms *b*, *c*, and *A* versus *s* are shown in Figure 4 for $R_0 = 2.75mm$ and $a = 6mm$. The terms *A* and *c* decrease linearly with the increase of *s*, while the constant *b* has an opposite behavior.

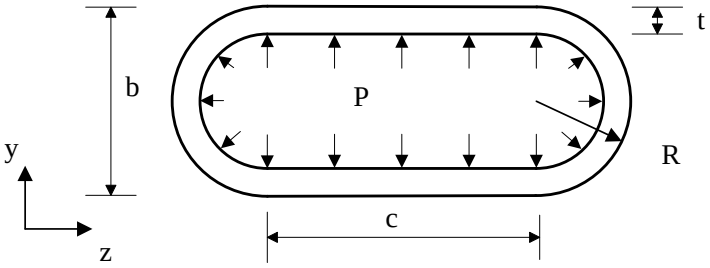

Figure 3. Geometry of a compressed tube

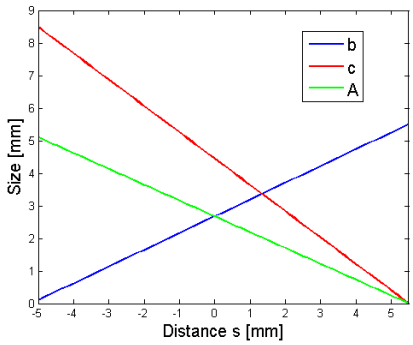

Figure 4. Distances between the upper and lower surfaces versus the internal height of the tube cell

3.2 Mechanical Model

The recovery force in y direction provided by the tube is considered with consisting in two parts (shown in Figure 5), one referring to the compressed circular configuration of the tube itself (F_R), the other one being related to the sum of the force in y direction caused by the elongation stress of the tube along its axial direction (F_S).

According to the Saint-Venant's principle [31], the shearing force on the two sides of the semicircle creates a moment *M* about x direction (Figure 6):

$$M = F_t \rho \tag{8}$$

Where $\rho = \frac{b-t}{2}$, while the original central radius of the semicircle is $\rho_0 = R_0 - \frac{t}{2}$.

Assuming pure bending occurring within the walls of the tube, the moment can be represented as:

$$M = \frac{1}{\rho} EI \tag{9}$$

Where the moment of inertia about x axis is $I = \frac{wt^3}{12}$, for the compressed structure shown in Figure 2, $w = 30mm$.

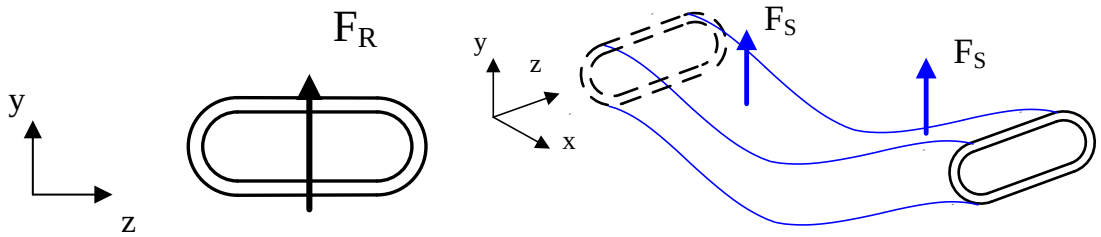

Figure 5. Schematic of F_R and F_S

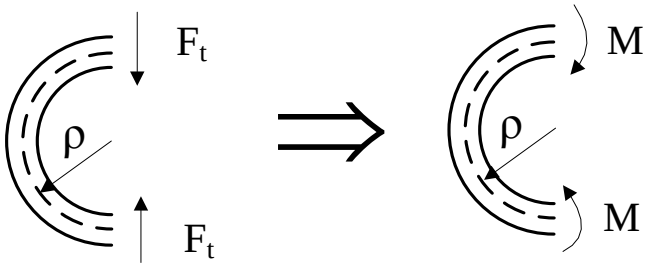

Figure 6. Mechanical model of semicircle

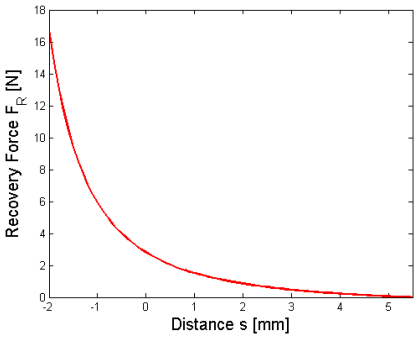

Figure 7. Curves of s versus F_R

The original shape of the tube is circular, which implies the presence of an internal pre-stress. Therefore the recovery force F_R of the tube should be composed by the shearing force, minus the original shearing force present in the two semicircles. From inspecting Figure 4, the relationship between F_R and s can be calculated and shown in Figure 7.

$$F_R = 2(F_t - F_{t0}) = 8EI\left(\frac{1}{(b-t)^2} - \frac{1}{(2R_0 - t)^2}\right) \tag{10}$$

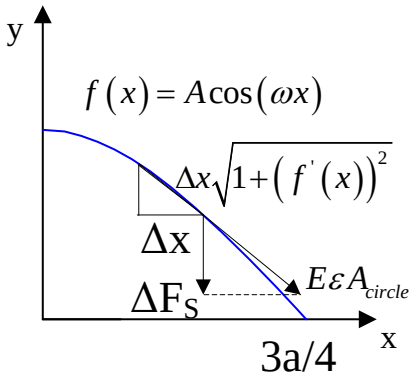

Figure 8. Principle of the recovery force F_S

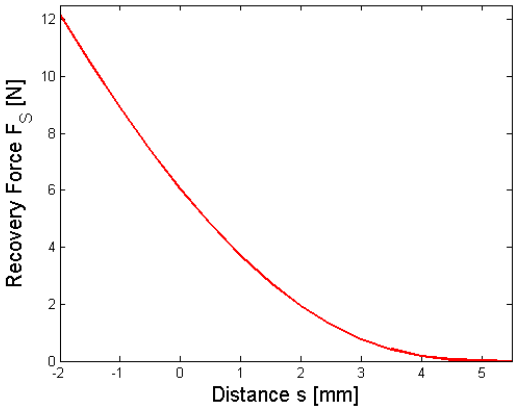

Figure 9. Curves of s versus F_S

The force F_S is given by the sum of the forces along the y-direction in each unit of the curve. Duo to the symmetry of the sinusoidal curve, we use the 1/4-period curve shown in Figure 8 to calculate the force F_S. The function of the blue curve is represented by:

$$f(x) = A\cos(\omega x) \tag{11}$$

From a horizontal straight line to sinusoidal curve, the strain at position x in a increment Δx is

$$\varepsilon = \frac{\Delta x\sqrt{1+\left(f'(x)\right)^2} - \Delta x}{\Delta x} = \sqrt{1+\left(f'(x)\right)^2} - 1 \tag{12}$$

So the force in y direction is

$$\Delta F_S = E\varepsilon A_{circle}\frac{f'(x)}{\sqrt{1+\left(f'(x)\right)^2}} \tag{13}$$

Here $A_{circle} = \pi\left(R_0{}^2 - \left(R_0 - t\right)^2\right)$.The resultant force F_S along the y-direction can be obtained from the following equation:

$$F_S = \int_0^{\frac{3a}{4}} \Delta F_S dx \tag{14}$$

The relation between the shearing force F_S and the distance s is shown in Figure 9.

4. Experiments

A prototype of the morphing structure was fabricated used as a hexagonal cellular structure made from 0.1 mm thickness steel with 6mm length of side, and filled with PU foam (Polycell Expanding Foam Polyfilla, Slough, UK, density: 15~130 kg/m3). The upper and lower honeycomb structures are connected by sandwiching two parallel tubes (PVC, Shenzhen Longxiang Electronic co., LTD. Outside radius R0: 2.75mm, thickness *t*: 0.84mm, valid length *L*: 30mm). Tensile tests carried out on the PVC tubes indicated a Young's modulus of the PVC material equal to *E*=0.94MPa. The morphing demonstrator was subjected to compressive loading using a tensile machine (SHIMADZU AGS-X, Shimadzu Corp., Kyoto, Japan, maximum force: 1000N) with a speed of 1mm/min. Force-displacement curves for the four samples produced are shown in Figure 10. The curves show a good level of repeatability, following approximately a quadratic dependence with the cross-bar displacement. Fluctuations are present between 3.5mm and 4.5mm due to possible contact or friction occurring between the upper and lower surface of the tubes.

Figure 11 shows the output force of the system versus the tubes input pressure at different positions of the crosshead. At constant imposed displacements, the measurements were taken in such a way that the force sensor was reset to zero to exclude the influence of the recovery force within the tubes. Figure 11 states a linear relationship between the input pressure and output force.

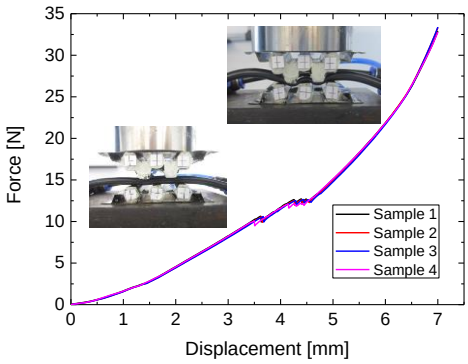

Figure 10. Curves of force versus displacement in compressing test

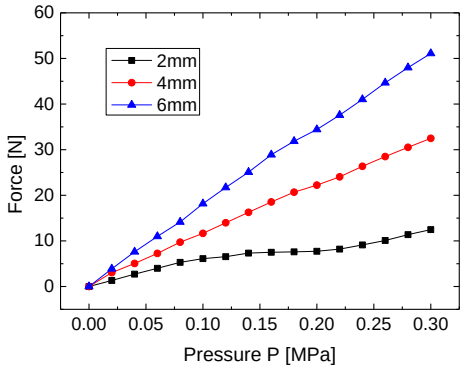

Figure 11. Output force versus the input pressure at different constant displacements

Another set of tests was conducted by imposing a constant load to the composite cellular core/inflatable tube systems (Figure 12(a)). The lower part of the honeycomb was fixed, and the loading was applied with a weight on the upper surface. The displacements were measured through image data processing tracking the deformation of six markers. The images were recorded using a camera (Canon Inc., Tokyo, Japan, number of pixels: 16 million), with a precision of 0.27 mm. The average distances measured between the upper and lower honeycomb are shown in Figure 12(b). At the conditions of 2kg loading and 0.4 MPa input pressure, the displacement of upper surface could reach 2.72mm.

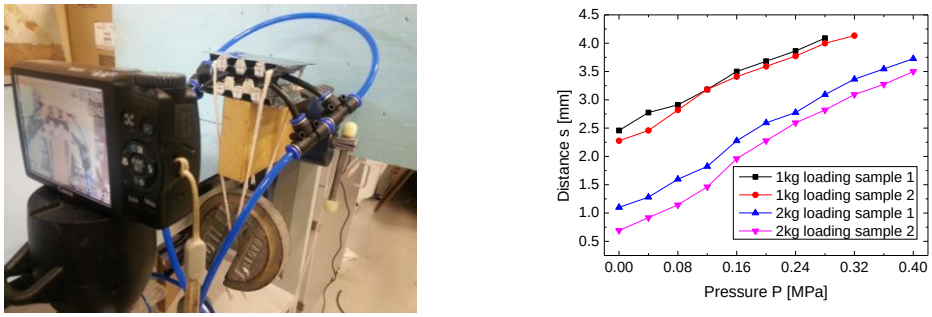

(a) (b)

Figure 12. Inflating test with weigh loading. (a) setup of the test rig; (b) displacement/pressure results

5. Results and discussions

The output force caused by the input pressure can be defined as:

$$F_P = PLc \tag{15}$$

In the case of the demonstrators built in this work, $L = 30mm$.

Figure 13 shows the relationship of the input pressure versus the output force. For *s*=3.5mm, the experimental results show a good agreement with the ones generated from the model. At smaller displacements (s=1.5mm and 0.5mm) the model tends to be conservative, especially for higher input pressures. It is worth mentioning that the model neglexts the expansion of the tune, which makes the term *c* larger than the one predicted by the model, and therefore leads to a larger output force.

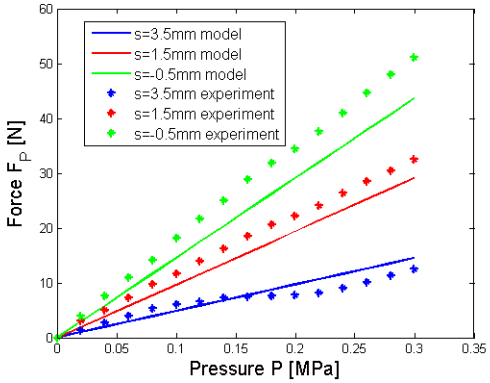

Figure 13. Output force versus input pressure provided by the model and the experimental demonstrator

When the morphing structure is compressed (as shown in Figure 10), the force measured by the force sensor equals the recovery force of the tubes. From Figure 2, there are two sinusoidal waves. The deformation conditions of left and right sides of a tube are free, so only the middle 1/2 period of the tube is elongated which is also verified in Figure 10.Therefore the recovery caused by the stress in one tube is $2F_S$. Because of the presence of two tubes in the system, the recovery force is $2F_R+4F_S$. From equations (10) and (12), the relationship between the distance between the upper and lower honeycomb surfaces and the recovery force is shown in Figure 14, together with the analogous curve from the experimental results. While s>2, the modelling value is smaller than the experimental one. In the model, we assume there are no

contact inside the tube, and no sliding between the tube and honeycomb. However, there occurs contact at *s*=2 with the reduction of *s*. Therefore, while s<2, the modelling value becomes bigger.

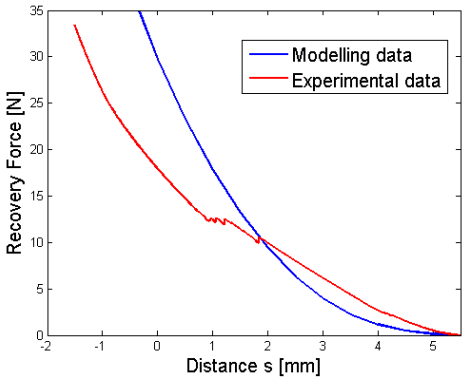

Figure 14. Recovery force versus distance between upper and lower honeycomb surfaces

From the balance of the forces in y direction under a vertical loading *G*, the following equation can be obtained.

$$2F_R + 2F_S + F_P = G \tag{16}$$

Under a prescribed external loading G, the distance between the upper and lower honeycomb surfaces at different input pressures can be calculated using equation (14). A comparison between the results from Equation (14) and the experimental measured data is shown in Figure 15. Especially for the lowest external load applied (1 Kg), one can observe an excellent agreement between the theoretical and tests results.

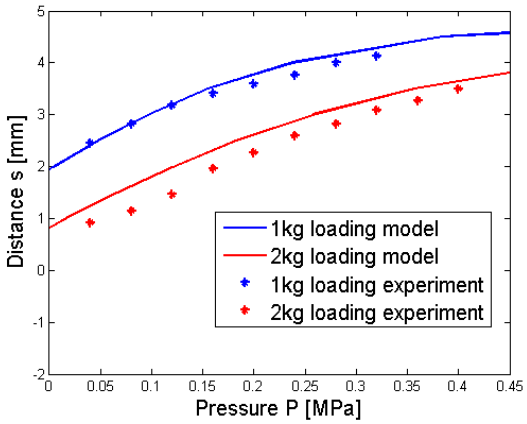

Figure 15. Distance between upper and lower honeycomb surface versus input pressure from the model and the experimental prototype

A prototype of a reduced-scale model of a morphing thickness airfoil (original airfoil: NACA0030) was fabricated with a chord of 140mm and maximum initial thickness of 43 mm. Using a similar manufacturing process to the one adopted for the composite cellular demonstrator, an airfoil was made using a 0.1mm thickness steel honeycomb, with PU expanding foam filler injected into the cellular structure and on the rest of the wingbox. After curing for 24h at room temperature, the final prototype was finished by cutting manually any extra polymer debording from the wingbox. Two parallel tubes were installed between the upper and lower honeycomb. Rubber bands were used to apply the loading on the wing structure. Figure 16 shows the vertical locations of points A1 (maximum thickness) and A2 on the

top of the wing, which increase with the input pressure. A thickness change of 7.6% (3.28mm) at point A1 can be obtained for a 0.28 MPa input. A demonstration of the morphing processing under different input pressures is shown in Figure 17.

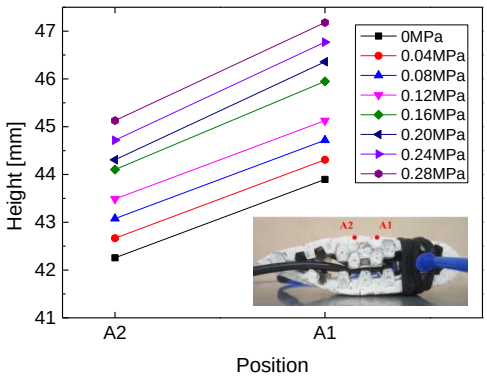

Figure 16. Heights morphing wing airfoil

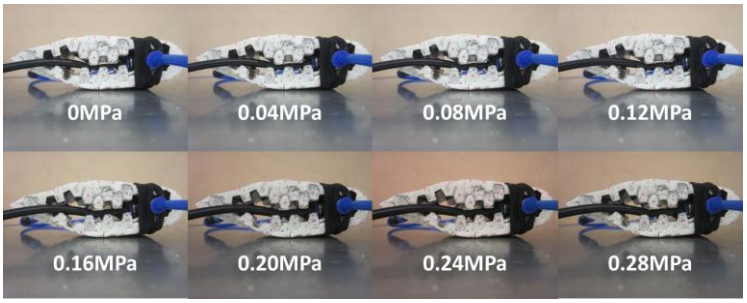

Figure 17. Morphing processing of the prototype under different input pressure

Conclusions

This paper has described the concept of a morphing thickness airfoil based on Pneumatic Flexible Tubes and cellular wingbox structure. An analytical model has been developed to calculate pressure/thickness relations and the mechanics of the actuation system. An experimental prototype of the composite cellular/inflatable tube structure has been manufactured and tested. The experimental and analytical results showed a good agreement, indicating that the model can be used as initial design tool. A prototype of a reduced-scale morphing thickness airfoil has also been fabricated and showed the feasibility of further exploring this concept as an alternative morphing wing strategy.

ACKNOWLEDGMENTS

This work is supported by the National Natural Science Foundation of China (Grant No.11225211, No.11272106). J. Sun would also like to thank CSC (Chinese Scholarship Council) for funding his research work at the University of Bristol. FS is also grateful to the European Commission for the FP7-AAT-2012-RTD-L0-341509 project that provides the infrastructure logistics of the activities described in this paper.

REFERENCES

1. Jha, A. K. and Kudva, J. N., "Morphing Aircraft Concepts, Classifications, and Challenges," In: *Proceedings of SPIE Vol. 5388,* Smart Structures and Materials 2004: Industrial and Commercial Applications of Smart Structures Technologies, pp. 213-224.
2. Roth, B., Peters, C., Crossley, W. A., "Aircraft Sizing with Morphing as An Independent Variable: Motivation, Strategies and Investigations," In: *AIAA's Aircraft Technology, Integration, and Operations (ATIO) 2002 Technical*, 1-3 October 2002, Los Angeles, California, AIAA 2002-5840.
3. Frommer, J. B. and Crossley, W. A., "Enabling Continuous Optimization for Sizing Morphing Aircraft Concepts," In: *43rd AIAA Aerospace Sciences Meeting and Exhibit*, 10-13 January 2005, Reno, Nevada. AIAA 2005-816.
4. Barbarino, S., Bilgen, O., Ajaj, R. M., Friswell, M. I. and Inman, D. J., A Review of Morphing Aircraft," *Journal of Intelligent Material Systems and Structures*, Vol. 22, 2011, pp. 823-877.
5. Gomez, J. C. and Garcia, E., "Morphing Unmanned Aerial Vehicles," *Smart Materials and Structures*, Vol. 20, 2011, 1030.01.
6. Rodriguez A. R., "Morphing Aircraft Technology Survey," In: *45th AIAA Aerospace Sciences Meeting and Exhibit*, 8 - 11 January 2007, Reno, Nevada. AIAA 2007-1258.
7. Secanell, M., Suleman, A. and Gamboa, P., "Design of a Morphing Airfoil Using Aerodynamic Shape Optimization," AIAA Journal, Vol. 44, No. 7, 2006, pp. 1550-1562.
8. Yu, M., Wang, Z. J. and Hu H, "Airfoil Thickness Effects on the Thrust Generation of Plunging Airfoils," *Journal of Aircraft*, Vol. 49, No. 5, 2012, pp. 1434-1439.
9. Ashraf, M. A., Young, J. and Lai, J. C. S., "Reynolds number, thickness and camber effects on flapping airfoil propulsion," *Journal of Fluids and Structures*, Vol. 27, 2011, pp. 145-160.
10. Ahaus, L., Roe, R., Peters, D. A. and Rong, X., "Representation of Morphing Airfoil Thickness in Dynamic Stall Simulations," In: *30th AIAA Applied Aerodynamics Conference*, 25 - 28 June 2012, New Orleans, Louisiana. AIAA 2012-2769.
11. Brailovski, V., Terriault, P., Georges, T. and Coutu, D., "SMA Actuators for Morphing Wings," *Physics Procedia*, Vol. 10, 2010, pp. 197-203.
12. Martin, J, Heyder-Bruckner, J. J., Remillat, C., Scarpa, F., Potter, K. and Ruzzene, M., "The hexachiral prismatic wingbox concept," *Physica Status Solidi (b)*, Vol. 245, No. 3, 2008, pp. 570-577
13. Bettini, P., Airoldi, A., Sala, G., Di Landro, L., Ruzzene, M. and Spadoni, A., "Composite chiral structures for morphing airfoils: Numerical analyses and development of a manufacturing process," *Composites Part B: Engineering*, Vol. 41, No. 2, 2010, pp.133-147.
14. Olympio, K. R. and Gandhi, F., "Zero Poisson's Ratio Cellular Honeycombs for Flex Skins Undergoing One-Dimensional Morphing," *Journal of Intelligent Material Systems and Structures*, Vol. 21, No. 17, 2010, pp.1737-1753
15. Hassan, M. R., Scarpa, F., Ruzzene, M. and Mohammed, N. A., "Smart Shape Memory Alloy Chiral Honeycomb," *Materials Science and Engineering A*, Vol. 481, 2008, pp. 654-657.
16. Okabe, Y. and Sugiyama, H., "Shape variable sandwich structure with SMA honeycomb core and CFRP skins," In: *Proceeding of SPIE Active and Passive Smart Structures and Integrated Systems 2009*, 728817.
17. Perkins, D. A., Reed, J. L. and Havens, Jr., "Morphing Wing Structures for Loitering Air Vehicles," In: *45th AIAA/ASME/ASCE/AHS/ASC Structures, Structural Dynamics & Materials Conference*, 19-22 April 2004, Palm Springs, California, AIAA 2004-1888.
18. Vos, R. and Barrett, R., "Mechanics of Pressure-Adaptive Honeycomb and its Application to Wing Morphing," *Smart Materials and Structures*, Vol. 20, 2011. 094010.
19. Pagitz, M., Lamacchia, E. and Hol, J., "Pressure-actuated Cellular Structures," *Bioinspiration and Biomimetics*, Vol. 7, 2012, 016007.

20. Pagitz, M. and Bold, J., "Shape-changing Shell-like Structures," *Bioinspiration and Biomimetics*, Vol. 8, 2013, 016010.
21. Schulz, S., Pylatiuk, C., Reischl, M., Martin, J., Mikut, R. and Bretthauer, G., "A Hydraulically Driven Multifunctional Prosthetic Hand," *Robotica*, Vol. 23, 2005, pp. 293-299.
22. Berring, J., Kianfar, K., Lira, C., Menon, C. and Scarpa, F., "A Smart Hydraulic Joint for Future Implementation in Robotic Structures," *Robotica*, Vol. 28, No. 07, 2010, pp. 1045-1056.
23. Menon, C. and Lira, C., "Active Articulation for Future Space Applications Inspired by the Hydraulic System of Spiders," *Bioinspiration and Biomimetics*, Vol. 1, 2006, pp. 52-61.
24. Lira, C., Menon, C., Kianfar, K. and Scarpa, F., "Bioinspired Hydraulic Joint for Highly Redundant Robotic Platforms," In: *ASME/IFToMM International Conference on Reconfigurable Mechanisms and Robots*, 2009, pp. 434-438.
25. Chang, B., Chew, A., Naghshineh, N. and Menon, C., "A Spatial Bending Fluidic Actuator: Fabrication and Quasi-Static Characteristics," *Smart Materials and Structures*, Vol. 21, 2012, 045008.
26. Mazlouman, S. J., Chang, B., Mahanfar, A., Vaughan, R. G., and Menon, C., "Beam-Steering Antenna using Bending Fluidic Actuators," *IEEE Transactions on Antennas and Propagation*, Vol. 61, No. 10, 2013, pp. 5287-5290.
27. Nojima, T. and Saito, K., "Development of Newly Designed Ultra-Light Core Structures," *JSME International Journal Series A*, Vol. 49, No. 1, 2006, pp. 38-42.
28. Saito, K., Agnese, F. and Scarpa, F., "A Cellular Kirigami Morphing Wingbox Concept," *Journal of Intelligent Material Systems and Structures*, Vol. 22, No. 9, 2011, pp. 935-944.
29. Chen, Y. J., Scarpa, F., Remillat, C., Farrow, I., Liu, Y. J. and Leng, J. S., "Curved Kirigami SILICOMB cellular structures with zero Poisson's ratio for large deformations and morphing," *Journal of Intelligent Material Systems and Structures*, 2013, DOI: 10.1177/1045389X13502852.
30. Virk, K., Monti, A., Trehard, T., Marsh, M., Hazra, K., Boba, K., Remillat, C. D. L., Scarpa, F. and I. R. Farrow, "SILICOMB PEEK Kirigami cellular structures: mechanical response and energy dissipation through zero and negative stiffness," *Smart Materials and Structures*, Vol. 22, No. 8, 2013, 084014.
31. Gregory, R. D. and Wan, F. Y. M., "On Plate Theories and Saint-Venant'S Principle," *International Journal of Solids and Structures*, Vol. 21, No. 10, 1985, pp. 1005-1024